Journal of Atmospheric Chemistry **4** (1986), 277 –291.

Quantum Yields for the Photodissociation of Acetone in Air and an Estimate for the Life Time of Acetone in the Lower Troposphere

H. MEYRAHN, J. PAULY, W. SCHNEIDER, and P. WARNECK
Max-Planck-Institut für Chemie, Postfach 3060, 6500 Mainz, F. R. Germany

(Received: 2 July 1985; in revised form: 26 November 1985)

Abstract. The room-temperature photodecomposition of acetone diluted with synthetic air was studied at nine wavelengths in the spectral region 250–330 nm. The quantum yields for the products CO_2 and CO indicated that it was not possible to suppress secondary reactions sufficiently, even with acetone/air mixing ratios as low as 150 ppmv, to derive from these data primary acetone photodissociation quantum yields. The behavior of CO_2 and CO formation nevertheless provides some insight into the mechanism of acetone photodecomposition. When small amounts of NO_2 are added to acetone/air mixtures, peroxyacetyl nitrate (PAN) is formed. Quantum yields for PAN are reported. They are better suited to represent primary quantum yields for acetone photodissociation, because PAN is a direct indicator for the formation of acetyl radicals. The data were combined with absorption cross-sections for acetone measured at wavelengths up to 360 nm to calculate photodissociation coefficients applicable to the ground-level atmosphere at 40° northern latitude. Comparison with the rates for the reaction of acetone with OH radicals shows that both processes contribute almost equally to the total acetone losses in the lower atmosphere. The resulting atmospheric life time at 40° northern latitude is 32 days, on average. This value must be considered an upper limit, since it does not take into account acetone losses due to the reaction of excited triplet acetone with oxygen.

Key words. Acetone, peroxyacetyl nitrate, acetone photo-oxidation, photodissociation coefficients, tropospheric life time.

1. Introduction

The presence of acetone in the atmosphere with volume mixing ratios of about 0.5 ppb (Penkett, 1982) is thought to arise largely from the balance between acetone production in the photo-oxidation of propane, and acetone losses due to photodecomposition by sunlight and reaction with OH radicals (Singh and Hanst, 1982). The second process is known, and the third suspected to generate acetyl radicals which in the air first attach oxygen and then nitrogen dioxide to yield peroxyacetyl nitrate (PAN) as the final product. Thus, acetone has been identified as an important precursor of PAN in the remote atmosphere. For a better understanding of this relationship, it is necessary to quantify the rates of the individual processes with the help of appropriate laboratory experiments. The present paper deals with the photolysis of acetone under simulated atmospheric conditions. We report quantum yields for the products CO_2, CO and PAN as a wavelength function between 250 and 330 nm. These data are then used to calculate acetone photo-

dissociation coefficients for atmospheric conditions existing in the vicinity of the Earth's surface.

The photochemistry of acetone has been studied extensively in the past and reviews are available (Noyes *et al.*, 1956; Cundall and Davies, 1967; Hoare and Pearson, 1963; Lee and Lewis, 1980). Most of the data were taken at elevated temperatures with the radiation centered at 313 nm. At 130°C, every excited acetone molecule decomposes to give CO and two methyl radicals. When oxygen is added, CO_2 becomes a major product. Comparatively few studies of acetone photo-oxidation were done at or near room temperature. The results are summarized in Table I. For later reference, we list in Table II the reactions expected to result from the photo-dissociation of acetone if secondary reactions of radicals with acetone and stable photolytic products are negligible. In the spectral region considered, acetone absorbs radiation primarily into the first excited singlet state S_1. Inter-system crossing then transfers a portion of the excitation energy to other states. Both, highly excited vibronic levels of the S_0 ground state and the T_1 triplet state are thus populated. The yield of triplet excitation is nearly unity at 313 nm but decreases as the wavelength is lowered. Singlet and triplet excitation are not distinguished in Table II, but the discussion will show that it is mainly singlet acetone which is subject to dissociation. Fluorescence and phosphorescence quantum yields are small and can be ignored in the present context.

The present study was begun with the notion that acetone concentrations in air and photochemical conversions can be kept sufficiently low to avoid the occurrence of secondary reactions involving acetone. If these conditions are met, CO_2 is formed entirely from the oxidation of thermalized acetyl radicals, while CO arises from the breakup of

Table I. Average quantum yields for CO_2 (CO in parentheses) reported by various investigators for the photo-oxidation of acetone at or near room temperature.

Authors	T (°C)	P_{ac} (kPa)	P_{O_2} (kPa)	P_{total} (kPa)	Wavelength (nm) 254	280	290	299	313
Marcotte & Noyes (1951)	25	17.5	0.033	17.5	–	–	–	–	0.2 (0.04)
Osborne *et al.* (1961)	30	5.6	26.7	32.3	–	–	–	–	0.55 (0.10)
Kirk & Porter (1962)	25	9.6	0.133	97.3	–	0.72 (0.14)	–	–	0.21 (0.025)
Pearson (1963)	36	19.3	0.02–0.09	19.3	1.65 (0.46)	–	–	–	0.21 (0.07)
Foley & Sidebottom (1982)	28	0.13–13.3	2.7	101	–	0.48	–	–	0.13
Gardner *et al.* (1984)	25	0.05	18.7	93.3	–	0.074	0.080	0.076	0.074

Table II. Reactions expected to occur in the photo-oxidation of acetone in air

Number	Reaction	Rate Coefficient[a] (cm^3/molecule s)
(1)	$CH_3COCH_3 + h\nu \longrightarrow CH_3COCH_3^*$	
(2)	$CH_3COCH_3^* + M \longrightarrow CH_3COCH_3$	
(3)	$CH_3COCH_3^* \longrightarrow CH_3 + CH_3CO$	
(4)	$\longrightarrow CH_3 + CH_3CO^*$	
(5)	$CH_3CO^* + M \longrightarrow CH_3CO$	
(6)	$CH_3CO^* \longrightarrow CH_3 + CO$	
(7)	$CH_3 + O_2 + M \longrightarrow CH_3O_2 + M$	fast
(8)	$CH_3CO + O_2 + M \longrightarrow CH_3(CO)O_2 + M$	fast
(9a)	$2\,CH_3O_2 \longrightarrow 2\,CH_3O + O_2$	1.5×10^{-13}
(9b)	$\longrightarrow HCHO + CH_3OH + O_2$	3.1×10^{-13}
(9c)	$\longrightarrow CH_3OOCH_3 + O_2$	
(10)	$2\,CH_3(CO)O_2 \longrightarrow 2\,CH_3 + 2\,CO_2 + O_2$	2.5×10^{-12}
(11)	$CH_3O_2 + CH_3(CO)O_2 \longrightarrow CH_3 + CO_2 + CH_3O + O_2$	3.0×10^{-12}
(12)	$CH_3O + O_2 \longrightarrow HO_2 + HCHO$	1.5×10^{-15}
(13)	$CH_3O_2 + HO_2 \longrightarrow CH_3OOH + O_2$	6.5×10^{-12}
(14)	$CH_3(CO)O_2 + HO_2 \longrightarrow CH_3(CO)OOH + O_2$	5×10^{-12}
(15)	$HO_2 + HO_2 \longrightarrow H_2O_2 + O_2$	2.5×10^{-12}
(16)	$CH_3O_2 + NO_2 \rightleftharpoons CH_3OONO_2$	
(17)	$CH_3(CO)O_2 + NO_2 \rightleftharpoons CH_3(CO)OONO_2$	
(18)	$CH_3O + NO_2 \longrightarrow CH_3ONO_2$	
(19)	$HO_2 + NO_2 \rightleftharpoons HOONO_2$	

[a] Addison *et al.* (1980), Baulch *et al.* (1982).

vitrationally-hot acetyl radicals. The quantum yields for CO_2 and CO would then provide a measure for primary acetyl formation.

Contrary to expectation, we were unable to suppress secondary reactions sufficiently, even when employing very low concentrations of acetone. We then explored the use of NO_2 as a scavenger for peroxyacetyl radicals and found that the formation of PAN may serve as a convenient indicator for the primary acetyl quantum yield. Table II includes the scavenging reactions expected to take place when minor concentrations of NO_2 are added to the chemical system.

2. Experimental Procedures

The photolysis apparatus was similar to one described in some detail previously (Moortgat and Warneck, 1979). The main element of the optical train were a xenon arc lamp, an f/2 monochromator followed by a refocussing lens, a cylindrical quartz photolysis cell of 10 cm length and 1.8 cm internal diameter, and a calibrated thermopile for monitoring the transmitted radiation. The monochromator was set to a spectral resolution of 5 nm at half-width. Photolyses were carried out under optically-thin conditions mainly with mixtures of 150–200 ppmv of acetone in synthetic air or similar mixtures containing

an additional 120 ppbv of NO_2. The gas mixtures were prepared in a mercury and grease-free gas handling system also described previously. For each experiment the mixture was expanded simultaneously into three identical, evacuated quartz cells. The content of the first cell was used to check on the purity of the gas mixture, the second cell was irradiated, and the third one was kept in the dark during the photolysis period to provide a blank. Irradiated and blank samples were analysed for CO_2 and CO when NO_2 was absent, and for PAN when NO_2 had been added, using gas chromatographic techniques. Separation of CO_2 and CO was achieved on columns packed with Poropak Q (60–80 mesh) and molecular sieve 5 Å (60–80 mesh), respectively. The CO_2 and CO were subsequently reduced to CH_4 by means of a nickel catalyst in the presence of hydrogen which enabled us to detect these substances with a flame ionization detector. A standard mixture of CH_4, CO_2 and CO in nitrogen was employed for calibration. Concentrations of PAN were determined with an O_3–NO chemiluminescence detector of our own design (Helas *et al.*, 1981). The instrument was fitted with a 25 cm glass column packed with Carbowax 400 on Diatomite CQ (100–120 mesh) in order to separate PAN from NO_2 and NO. After its passage through the column, PAN was thermally decomposed and converted to NO in a tube filled with molybdenum chips heated to 360°C. The conversion efficiency was better 95%. The chemiluminescence resulting from the reaction of ozone with NO was picked up by a photomultiplier and the signal recorded with a pulse counter/rate meter. The signal was optimized by reducing the nitrogen carrier gas flow to 80 cc/min. Instrument calibration was performed with a mixture of 100 ppbv NO in nitrogen. Product quantum yields were calculated from the relation

$$\Phi(P) = \frac{m(P) \cdot V}{m(\mathrm{Ac}) \cdot \sigma \cdot I_0 \cdot A \cdot L \cdot \Delta t}$$

where V is the volume and L the length of the photolysis cell, σ is the absorption cross-section for acetone, I_0 is the photon flux and A the cross-section of the light beam in the photolysis cell, Δt is the irradiation time, $m(P)$ is the mixing ratio of accumulated product, and $m(\mathrm{Ac})$ is that of acetone. The photon flux was derived from the signal generated by the thermopile and the known calibration factor. In addition, acetone photolysis at 125°C (in the absence of oxygen) was employed for actinometry. At this temperature the CO quantum yield is unity. The results agreed with those obtained with the thermopile provided the reflection of light at the rear window of the photolysis cell was taken into account.

An adequate knowledge of acetone absorption cross-sections is essential for our method of determining quantum yields and for calculating photo-dissociation coefficients. Satisfactory data for the long wavelength tail of the acetone absorption band were not available. We have measured the needed cross-sections, using for this purpose a 0.6 m Czerny–Turner monochromator set to a resolution of 0.04 nm at halfwidth. The position of the grating was adjusted with a stepper motor. A tungsten filament lamp served as a background source. The signal from the photomultiplier detector was digitized and fed into a computer for storage and processing. Data from a number of runs were then computer-averaged. Absorption cells, placed between exit slit and detector, had lengths of 0.1 and

1 m. In addition, a 27 m pathlength was provided by a 1.2 m White cell. Acetone pressures ranged from 0.1 to 6.7 kPa.

3. Results

Absorption cross-sections for acetone are plotted in Figure 1 in two sections: from 275 to 330 nm, and from 330 to 360 nm. At longer wavelengths, the cross-sections are smaller than 2×10^{-23} cm^2/molecule. The spectrum is smooth in all regions investigated and shows no evidence of significant structure. Cross-sections for the determination of quantum yields were derived by averaging the high-resolution data over 3 nm wavelength intervals. The values are included in Table III. At the wavelengths 360, 350, and 340 nm the values are, respectively, 2.0, 3.2, and 11.3 in units of 10^{-23} cm^2.

Quantum yields were determined at nine wavelengths between 250 and 330 nm. Table III lists the average values obtained for the products CO_2 and CO in acetone/air mixtures at 100 kPa pressure. The variation with wavelength is displayed in Figure 2a. There are two noteworthy features. One is the rise of quantum yields with decreasing wavelength in the spectral region below 310 nm. Here, the CO/CO_2 ratios stay approximately constant (except perhaps at 250 nm), but the CO_2 quantum yield eventually reaches values greatly in excess of unity indicating the consumption of acetone by secondary reactions. The other feature is the minimum of quantum yields near 310 nm and the rise toward longer wavelengths. Thus, the region longward of 310 nm behaves differently from that at shorter wavelengths.

The pressure dependence of CO_2 quantum yields was explored at 300 nm with constant acetone/air mixing ratio. The results are shown in Figure 3 in the form of a Stern–Volmer plot. The data points fall on a straight line whose intercept with the ordinate suggests a low pressure CO_2 quantum yield of 1.35. The value is again significantly greater than unity so that secondary reactions must be involved even at 300 nm.

Table III. Experimental conditions and quantum yields for the formation of CO_2 and CO in the photo-oxidation of 150 ppmv acetone in air at 100 kPa total pressure

λ (nm)	σ (10^{-22} cm^2)	I_0 (10^{13} photons/cm^2 s)	Irrad. time (10^3 s)	I_{abs} (10^{11} photons/s)	n[a]	quantum yields CO_2	CO	$\phi CO/\phi CO_2$
250	237	54.6 ± 5.0	3.7–5.8	4.66 ± 0.42	7	1.59 ± 0.15	0.45 ± 0.08	0.28
260	366	89.9 ± 8.6	3.8–6.7	11.69 ± 0.13	7	1.40 ± 0.09	0.18 ± 0.05	0.13
270	463	133.7 ± 16.5	3.9–4.8	22.39 ± 0.28	7	1.15 ± 0.13	0.10 ± 0.02	0.09
280	505	181.2 ± 21.2	3.6–4.5	31.03 ± 0.36	6	0.86 ± 0.04	0.09 ± 0.01	0.10
290	421	238.0 ± 28.6	4.3–5.6	32.50 ± 0.46	8	0.61 ± 0.04	0.07 ± 0.01	0.10
300	278	315.8 ± 98.5	4.3–15.1	30.76 ± 0.96	8	0.27 ± 0.02	0.03 ± 0.03	0.11
310	144	349.7 ± 45.2	5.6–7.8	17.44 ± 0.22	14	0.11 ± 0.02	0.02 ± 0.01	0.18
320	48	263.7 ± 18.06	6.9–21.4	5.41 ± 0.37	11	0.18 ± 0.05	0.06 ± 0.05	0.33
330	8	278.3 ± 19.6	47.3–66.6	1.71 ± 0.12	7	0.27 ± 0.09	0.09 ± 0.03	0.34

[a] Number of experiments.

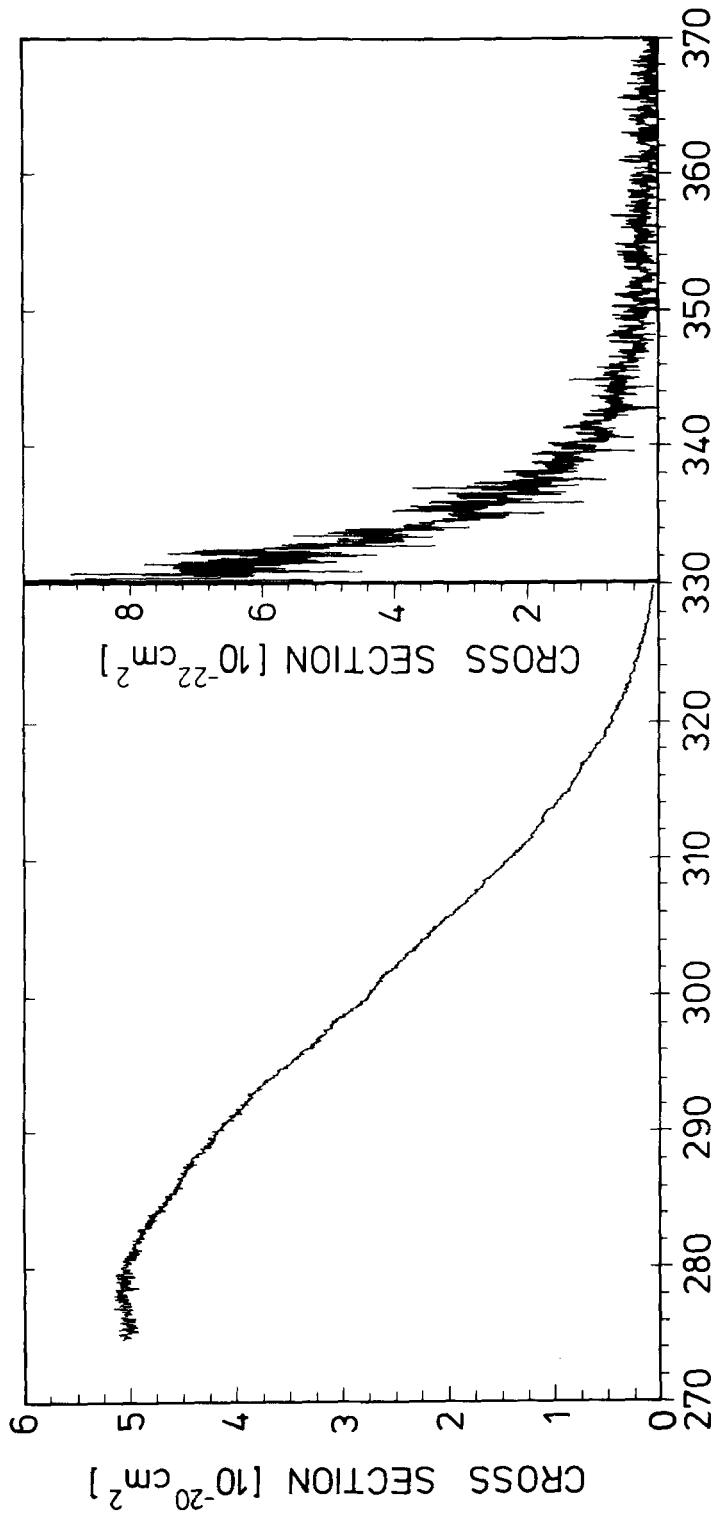

Fig. 1. Absorption cross-sections of acetone as a function of the wavelength. Resolution is 0.04 nm at halfwidth. Data shown are averages of five runs in the region 275–305 nm, of 14 runs in the region 305–325 nm, and of 2 runs in the region 325–360 nm.

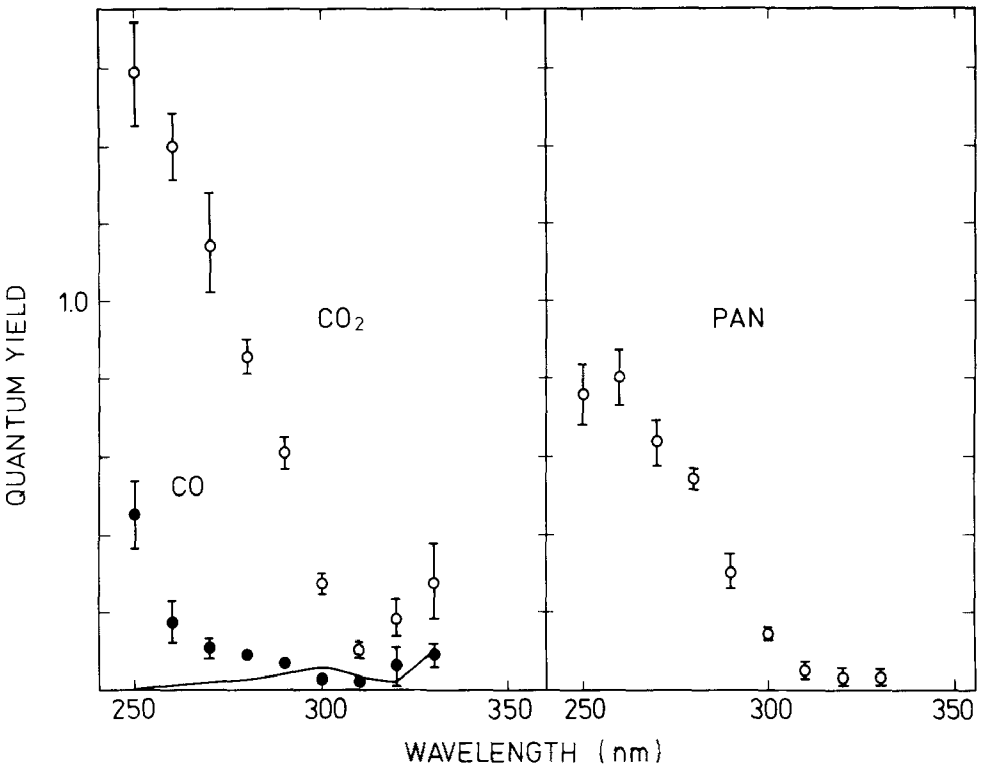

Fig. 2. Product quantum yields for the photodecomposition of acetone in air at 100 kPa total pressure as a function of wavelength. Left: CO_2 (open circles) and CO (points). Solid line describes CO quantum yields from the secondary photolysis of formaldehyde according to steady state calculations based on the reactions shown in Table II. Right: quantum yields for PAN in the presence of nitrogen dioxide.

Further evidence for the occurrence of secondary reactions was obtained by raising the acetone/air mixing ratio from 150 to 1000 ppmv in a few experiments, keeping the total pressure constant at 100 kPa. The effect was slight at 320 nm wavelength, whereas at 280 nm the CO_2 quantum yield increased significantly. It was not possible to work with mixing ratios substantially lower than 150 ppmv because of insufficient light absorption leading to inconveniently long photolysis times.

The formation of PAN in the presence of NO_2 was observed to rise essentially linearly with time until almost the entire supply of NO_2 became exhausted. In determining quantum yields the conversion of NO_2 was kept below 30%. As judged from the chromatograms, nitrogen-containing products other than PAN were unimportant. Quantum yields for PAN are shown in Figure 2b as a function of wavelength. The numerical data are given in Table IV. In the spectral region below 310 nm, the yield of PAN rises with decreasing wavelength similar to that of CO_2 in the absence of NO_2, but the values remain smaller than unity even at 250 nm indicating that NO_2 largely suppresses secondary reactions. At wavelengths longer than 310 nm the PAN quantum yields continue to decline and they do not follow the upturn evident in the CO_2 and CO quantum yields. The data

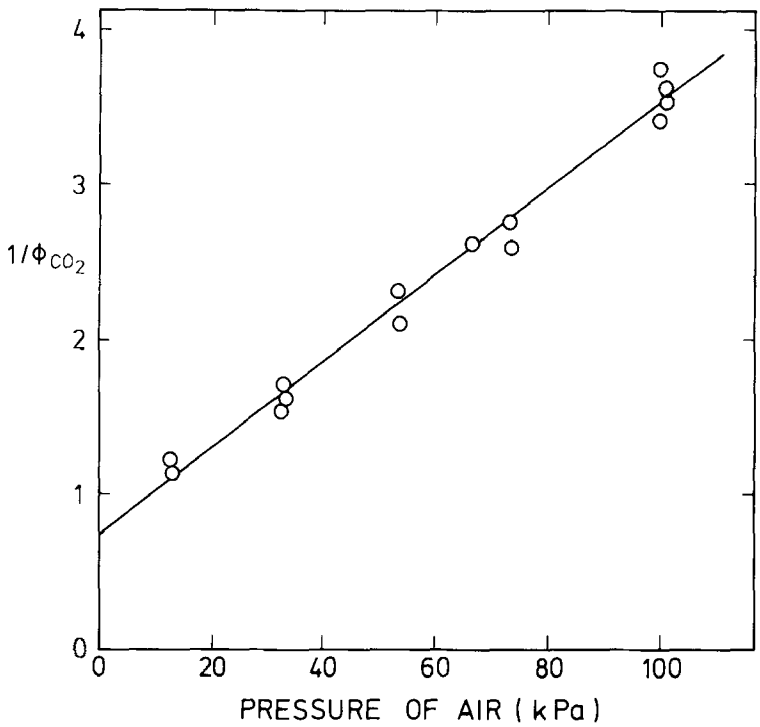

Fig. 3. Stern–Volmer plot of CO_2 quantum yields at 300 nm wavelength.

Table IV. Experimental conditions and quantum yields for the formation of PAN in the photooxidation of 200 ppmv acetone in air at 100 kPa total pressure in the presence of 120 ppbv NO_2

λ (nm)	σ (10^{-22} cm^2)	I_0 (10^{13} photons/cm^2 s)	Irrad. time (10^3 s)	I_{abs} (10^{11} photons/s)	n[a]	quantum yield (PAN)	ϕ_{CO_2}/ϕ_{PAN}
250	237	40.8 ± 3.2	0.25–0.79	4.8 ± 0.38	5	0.76 ± 0.08	2.09
260	366	61.0 ± 0.9	0.13–0.16	11.0 ± 0.10	3	0.80 ± 0.07	1.75
270	463	99.0 ± 5.6	0.06–0.24	22.6 ± 0.14	3	0.64 ± 0.05	1.79
280	505	144.0 ± 2.1	0.08–0.18	34.1 ± 0.70	3	0.55 ± 0.03	1.56
290	421	189.0 ± 0.7	0.06–0.25	37.2 ± 0.30	3	0.30 ± 0.05	2.03
300	278	236.0 ± 1.2	0.27–0.30	31.7 ± 0.30	3	0.15 ± 0.005	1.80
310	144	303.0 ± 2.5	0.55–1.19	22.3 ± 0.30	5	0.05 ± 0.02	2.20
320	48	341.0 ± 3.7	1.28–3.46	9.8 ± 0.20	5	0.028 ± 0.008	64.3
330	8	433.0 ± 4.9	1.09–6.9	1.9 ± 0.40	6	0.033 ± 0.011	81.8

[a] Number of experiments.

at 330 nm are less certain than the others. At this wavelength, the absorption cross-section for acetone becomes unfavorably small compared with that for NO_2 with the consequence that NO_2 may have been inadequately shielded against photolysis. At all other wavelengths the photolysis of NO_2 is negligible compared with that of acetone because the latter is present with 1000 fold excess. Table IV includes ratios of CO_2 to PAN quantum yields. The ratio is 1.89 ± 0.26, on average, in the region below 310 nm.

We have computed noon-time atmospheric photo-dissociation coefficients for acetone, applicable to the ground level atmosphere, by assuming that PAN quantum yields represent primary photo-dissociation quantum yields. The photo-dissociation coefficient then is defined by

$$j(\theta) = \Sigma_i \Phi_i \,(\mathrm{PAN})\, \sigma_i I_i(\theta)$$

where $I_i(\theta)$ is the global solar radiation flux (including scattered light) within the wavelength interval $\Delta\lambda_i$ for the solar zenith angle θ. Quantum yields and absorption cross-sections refer to the same wavelength interval and the summation ranges from 290 to 360 nm. Solar fluxes were taken from the compilation of Peterson (1976) for best estimate surface albedoes. These data refer to middle latitudes of the Northern Hemisphere. In the computations, an uncertainty arises from the lack of quantum yield data at wavelengths greater than 330 nm and our ignorance how the known values should be extrapolated. Therefore, two cases were constructed. The first assumes constant PAN quantum yields of 0.03 in the wavelengths region above 320 nm, the second case uses a linear extrapolation towards zero at wavelength between 320 and 340 nm. The resulting photo-dissociation coefficients are given in Table V. They represent upper- and lower-limit values. The computations show that the uncertainty of quantum yields at wavelengths greater than 330 nm affects the results very little. The major contribution to the integrated photo-dissociation rate evidently is due to solar radiation at wavelengths below 330 nm.

Table V. Photodissociation coefficients j for acetone in air at 100 kPa total pressure

Solar zenith angle	Limits	20°	30°	40°	50°	60°	70°
$j(10^{-7}\ s^{-1})$	lower	5.90	5.04	3.96	2.75	1.50	0.62
	upper	6.28	5.39	4.27	3.01	1.70	0.73

4. Discussion

4.1. *Spectrum*

Norrish *et al.* (1934) and Noyes *et al.* (1934) have reported on the presence of discrete structure in the absorption spectrum of acetone in the wavelength region 300–330 nm. These older experiments were done with the absorption tube placed in front of the spectrograph wich subjects acetone to photo-decomposition. One cannot, therefore, preclude the possibility that the structure detected was due in part to accumulated

photolytic products. No identifiable structure was observed in the present study. Our spectral resolution was similar in magnitude to that employed by Noyes *et al.* (1934). Yet the few undulations superimposed on the continuum in our spectra (below 330 nm) do not at all coincide with the wavenumber assignments for the discrete features reported by them. A discrete spectrum was formerly believed to be necessary to explain the fluorescence obtained at longer wavelengths. With a sufficient density of ro-vibronic levels in the upper state of acetone, however, the absorption spectrum would assume the appearance of a quasi-continuum due to the overlap of Doppler-broadened lines. It is conceivable that a higher spectral resolution may reveal discrete features, but even so the quasi-continuous absorption will be dominant.

4.2. *Quantum Yields*

The trend of rising CO_2 (and CO) quantum yields upon lowering the wavelength from 310 to 250 nm is in accord with most of the previous data (see Table I) except those of Gardner *et al.* (1984) who found little change between 313 and 280 nm. Their data disagree with ours also with respect to the pressure dependence in that their quantum yields do not follow a Stern–Volmer relationship. The discrepancy between both data sets is all the more perturbing as Gardner *et al.* are the only investigators who used experimental conditions very similar to ours (but note that Gardner *et al.* have determined other products in addition to CO_2 and found a reasonable carbon mass balance). The existence of a pressure effect nevertheless demonstrates the importance of collisional deactivation of photo-excited acetone. There can be no doubt that the low product quantum yields observed in the 290–320 nm wavelength region are the consequence of collisional quenching. To elucidate the quantitative details of the deactivation processes involved, however, requires further work.

The present study seems to be the first to have explored the wavelength region above 313 nm. Here, the photochemical behavior of acetone is different from that in the region below 310 nm. The unexpected dichotomy suggests the participation of two excited states and this possibility must be discussed. Although the $^1(n - \pi^*)$ transition represented by the 230–360 nm absorption band of acetone primarily excites the S_1 singlet state, internal energy conversion rapidly populates the lowest triplet state T_1 as well as highly excited vibronic levels of the S_0 ground state. Dissociation into CH_3 and CH_3CO is thought to occur from all three states.

The properties of the triplet state are characterized as follows. At 313 nm, a variety of measurements have demonstrated a high S_1–T_1 conversion efficiency of close to unity (Cundall and Davies, 1967). Heicklen (1959) has shown that the weak triplet emission (phosphorescence) declines in intensity as the wavelength is lowered from 313 to 280 nm and this observation is thought to indicate a decrease in the intersystem crossing yield. Oxygen is known to have a great capacity for quenching the triplet (but not the singlet) state. Two torr of oxygen suffice to remove essentially all the phosphorescence emission observed with 313 nm excitation. If the effect arises mainly from physical quenching, i.e., an energy transfer to the quenching molecule similar to that observed with biacetyl,

aliphatic aldehydes or alkenes (Rebbert and Ausloos, 1964; 1965), the triplet state would be so rapidly deactivated at atmospheric pressures of oxygen that its contribution to acetone photodecomposition becomes insignificant. Pearson (1963) and Kirk and Porter (1962) have also discussed the possibility that a portion of triplet acetone undergoes chemical reaction with oxygen to give CO_2 and CO as products. They found the evidence for the occurrence of such a process inconclusive at best.

In the wavelength region below 300 nm, the situation is fairly clear. Here, the triplet state is of minor importance and acetone decomposition must occur predominantly via the singlet states. PAN and CO_2 quantum yields both rise with decreasing wavelength indicating an increase in the rate of decomposition compared with that of collisional quenching when the excitation energy is raised. This behavior is in accordance with expectation. The situation concerning the wavelength region above 310 nm is less well understood. The low PAN quantum yields and the larger CO_2/PAN ratios show that the yield of acetyl radicals is very much reduced and that much of the CO_2 must be generated by a mechanism different from that taking place at shorter wavelengths. Since, furthermore, the triplet state is produced with a high yield (at least at 313 nm), our data suggests a reaction of triplet acetone with oxygen as the source of CO_2 (for CO vide infra). Following Pearson (1963), the reaction may be written

$$CH_3COCH_3(T_1) + O_2 \longrightarrow CH_3 + CH_3O + CO_2 \qquad (20)$$

The mechanistic details of the reaction are unknown, but acetyl radicals probably are not formed. The process would still have to compete with physical quenching in order to explain the relatively low CO_2 quantum yields.

Yet another problem encountered in the present study is the unexpected production of secondary CO_2 despite the low acetone/air mixing ratios employed. The CO_2/PAN ratio observed at wavelengths below 310 nm suggests that almost two CO_2 molecules are formed for each acetyl radical resulting from acetone photodecomposition. The excess CO_2 presumably arises in reactions of radicals with acetone. As Table II shows, the radicals arising from acetone photodissociation in the presence of oxygen are CH_3O_2, $CH_3(CO)O_2$, CH_3O and HO_2. Of these, CH_3O is the only one capable of abstracting a hydrogen atom from acetone in an exothermic reaction. Hydrogen abstraction by peroxy radicals is endothermic, by contrast, and must be negligibly slow. According to Table II, the CH_3O radical also reacts with oxygen and this reaction is favored under our experimental conditions. The reactions to be considered thus are

$$CH_3O + O_2 \longrightarrow CH_2O + HO_2 \qquad (12)$$

$$CH_3O + CH_3COCH_3 \longrightarrow CH_3OH + CH_2COCH_3 \qquad (21)$$

$$CH_2COCH_3 + O_2 \longrightarrow CH_2O + CO_2 + CH_3 \qquad (22)$$

where the last step summarizes CO_2 formation from the acetonyl radical according to the proposal of Pearson (1963). The rate coefficient for reaction (12) is $k_{12} = 1.5 \times 10^{-15}$ cm^3 molecule^{-1} s^{-1} at room temperature (Baulch *et al.*, 1982). The rate coefficient required to make reaction (21) important at atmospheric pressures of oxygen would have to be

$k_{21} = k_{12}(O_2)/(\text{acetone}) = 1 \times 10^{-12}$, a value that is unacceptably high. Firstly, the equivalent abstraction reaction of hydroxyl radicals has a rate coefficient (Zetzsch, 1982, Rhäsa *et al.*, 1985) almost one order of magnitude lower (2.3×10^{-13}), even though the reaction is, by 65 kJ/Mol, more exothermic. Secondly, the older literature reviewed by Gray *et al.* (1967) suggests an activation energy of about 25 kJ/Mol for the abstraction of a hydrogen atom from a methyl group by CH_3O and a pre-exponential factor of the order of 4×10^{-13} cm^3 $molecule^{-1}$ s^{-1}, which combines to give a room temperature value for k_{21} of 3×10^{-17}. The magnitude is too low to make the formation of acetonyl radicals by reaction (21) important under our experimental conditions. We are forced to conclude that excess CO_2 must be formed by another route.

It is possible that peroxy radicals may react with acetone by addition to the central carbon atom rather than by hydrogen abstraction in a manner that was recently found to be manifested in the reaction of HO_2 with aldehydes (Su *et al.*, 1979; Niki *et al.*, 1980; Veyret *et al.*, 1982). We have considered a number of conceivable reaction pathways but found all of them endothermic.

Yet another possibility for the formation of excess CO_2 is the generation of OH radicals by secondary photolysis of H_2O_2 produced in reaction (15) (and of CH_3OOH and $CH_3(CO)OOH$ produced in reactions (13) and (14), respectively), followed by the reaction of OH with acetone. In order to assess the importance of these processes a steady-state analysis was performed of the reaction mechanism given in Table II and average OH quantum yields were calculated as a function of the wavelength. The effect is most pronounced at wavelengths near 260 nm, but even here the OH quantum yields are smaller than 10% of those for PAN. The corresponding rate of OH production is insufficient to explain the excess of CO_2 unless the reaction of OH with acetone leads to a chain reaction in which OH radicals are regenerated. We have no knowledge about how this should happen. Thus, we are unable to suggest a reaction scheme which might explain the observed CO_2 quantum yields.

The same steady-state analysis was used to determine the amount of CO produced by the secondary photolysis of formaldehyde resulting from reactions (9a) and (12). The average CO quantum yields calculated are entered in Figure 2a to show that formaldehyde photolysis can explain the yield of CO observed in the spectral region above 290 nm, but not that at shorter wavelengths. It is likely that at least part of the additional CO production is due to the decomposition of vibrationally excited acetyl radicals, reaction (6) in Table II. The extent to which this reaction may contribute to total acetone photodissociation is given by the difference between the observed PAN quantum yields and unity. Indeed, at most wavelengths the difference is large enough to accommodate the CO quantum yield provided correction for formaldehyde photolysis is made. The CO quantum yield at 250 nm is an exception in that the sum of PAN and CO quantum yields becomes greater than unity. The excess may be due in part, or even entirely, to the much larger error margin. It is certainly more appealing to assign the formation of CO in this wavelength region to reaction (6) than to an unknown secondary chain reaction, although the latter possibility cannot be precluded on the basis of the available data.

Finally, it should be noted that in the atmosphere NO is present due to photolysis of

NO_2, and that NO competes with NO_2 for acetylperoxy radicals generated in reaction (8) of Table II:

$$NO + CH_3(CO)O_2 \longrightarrow CH_3 + CO_2 + NO_2 \quad (23)$$

This parallel reaction leads to a loss of acetylperoxy and PAN. In laboratory experiments designed to determine primary quantum yields of acetone photolysis it is not possible to utilize NO as a scavenger, and CO_2 as an indicator for acetylperoxy radicals because HO_2 radicals resulting from reaction (12) in Table II would then react with NO as well

$$NO + HO_2 \longrightarrow NO_2 + OH \quad (24)$$

thereby generating OH radicals. Their subsequent reaction with acetone would initiate a chain process leading to the formation of additional CO_2. As we pointed out in the introduction, such secondary reactions must be suppressed if primary quantum yields are to be derived from the yield of stable products.

Minor amounts of NO undoubtedly were present also in our experiments with NO_2 as scavenger. The NO_2 photolysis rate was much smaller, however, than that of acetone at all wavelengths except 330 nm. By taking into account that NO reacts not only with $CH_3(CO)O_2$ but also with CH_3O_2 radicals we estimate a reduction of PAN quantum yields due to reaction (23) of one percent, at most, of the values given. At 330 nm, as much as 25% of the acetylperoxy radicals may have reacted with NO. The PAN quantum yields of 330 nm should, accordingly, be considered as a lower limit.

4.3. *Photodissociation Coefficients*

The photodissociation coefficients in Table V are based on quantum yields for PAN as a convenient indicator for acetyl radical formation. The data do not take into account any reaction of excited acetone molecules with oxygen unless such a reaction leads also to the production of acetyl. The different behavior of CO_2 and PAN quantum yields at wavelengths greater than 310 nm shows, however, that the process forms CO_2 mainly by a route not involving acetyl radicals. Accordingly, these must originate primarily from the photodissociation of acetone, reaction (3) in Table II. The formation of hot acetyl radicals which decompose towards CO and CH_3 can be neglected at wavelengths greater than 290 nm. These remarks make clear that with regard to total acetone photodecomposition the data in Table V are minimum values because they neglect losses due to the reaction of excited acetone molecules with oxygen. Gardner *et al.* (1984) have used their quantum yield data to calculate total acetone loss rate constants. Their values are by a factor of about two higher than ours.

In order to estimate life times of acetone in the lower atmosphere resulting from photodissociation it is necessary to average the photodissociation rates over a full day including the dark hours. We have performed this exercise for conditions at 40° northern latitude using the second line of values in Table V. The results are given in Table VI for several seasons, namely January, July, and equinox. It is also of interest to compare the

Table VI. Acetone loss rates and atmospheric life times in the lower troposphere at 40° northern latitude

	January	Equinox	July	Annual average
Loss by photodissociation (s^{-1})	$3.3 \cdot 10^{-8}$	$1.0 \cdot 10^{-7}$	$1.8 \cdot 10^{-7}$	$1.0 \cdot 10^{-7}$
OH number density (molecules/cm^3)	$0.31 \cdot 10^{6}$	$1.18 \cdot 10^{6}$	$2.0 \cdot 10^{6}$	–
Loss by reaction with OH (s^{-1})	$6.8 \cdot 10^{-8}$	$2.6 \cdot 10^{-7}$	$4.4 \cdot 10^{-7}$	$2.6 \cdot 10^{-7}$
Total loss rate (s^{-1})	$1.0 \cdot 10^{-7}$	$3.6 \cdot 10^{-7}$	$6.2 \cdot 10^{-7}$	$3.6 \cdot 10^{-7}$
Lifetime (days)	114.4	31.9	18.6	31.9

rates with loss rates due to the reaction of acetone with OH radicals. The rate coefficient for this reaction is 2.2×10^{-13} cm^3 $molecule^{-1}$ s^{-1} at 298 K (Zetsch, 1982; Rhäsa *et al.*, 1985). Number densities for OH radicals were taken from an improved data set of Crutzen (1982). Table VI shows that both processes occur with rates comparable in magnitude. Photodissociation and reaction with OH radicals combined result in a life time of acetone in the ground level atmosphere of 32 days, on average, with shorter values in summer and longer ones in winter. Although the life times derived here must be considered upper limit values, they are long enough to subject acetone to transport in the lower atmosphere. Owing to the pressure-dependence of the quantum yields, the photodissociation coefficient is expected to increase with altitude, whereas the OH number density decreases, at least in the region of the troposphere. The rate coefficient for the reaction of acetone with OH also is expected to decrease, because of the temperature drop with increasing altitude in the troposphere. Roughly, therefore, we expect the tropospheric life time for acetone to be independent of height. There will be a pronounced dependence on latitude, however, with higher loss rates near the equator compared to those at the poles.

Acknowledgement

The present work was performed as part of the program of the Sonderforschungsbereich 73 (Atmospheric Trace Substances) and it has received support by the Deutsche Forschungsgemeinschaft.

References

Addison, M. C., Burrows, J. P., Cox, R. A., and Patrick, R., 1980, Absorption spectrum and kinetics of the acetylperoxy radical, *Chem. Phys. Lett.* 73, 283–287.

Baulch, D. L., Cox, R. A., Crutzen, P. J., Hampson, R. F. Jr., Kerr, J. A., Troe, J., and Watson, T. R., 1982, Evaluated kinetic and photochemical data for atmospheric chemistry; Supplement I CODATA task group on chemical kinetics, *J. Phys. Chem. Ref. Data* 11, 327–496.

Crutzen, P. J., 1982, The global distribution of hydroxyl, in E. D. Goldberg (ed.) *Atmospheric Chemistry, Dahlem Konferenzen*, Springer-Verlag, Berlin, pp. 313–328.

Cundall, R. B. and Davies, A. S., 1967, Primary processes in the gas phase photochemistry of carbonyl compounds, *Progr. Reaction Kinet.* 4, 149–213.

Foley, M. B., and Sidebottom, H. W., 1982, Reactions of the triplet state of ketones with molecular oxygen, in B. Versino and H. Ott (eds.) *Proc. 2nd European Symp. Physico-Chemical Behaviour of Atmospheric Pollutants*, D. Reidel, Dordrecht, Holland, pp. 165–171.

Gardner, E. P., Wijayaratne, R. D., and Calvert, J. G., 1984, Primary quantum yields of the photodecomposition of acetone in air under tropospheric conditions, *J. Phys. Chem.* 88, 5069–5076.

Gray, P., Shaw, R., and Thynne, J. C. J., 1967, The rate constants of alkoxy radical reactions, *Progr. Reaction Kinet.* 4, 63–117.

Helas, G., Flanz, M., and Warneck, P., 1981, Improved NO_x monitor for measurements in tropospheric clean air regions, *Intern. J. Environ. Anal. Chem.* 10, 155–166.

Hoare, D. E. and Pearson, G. S., 1963, Gaseous photooxidation reactions, *Adv. Photochem.* 3, 83–156.

Heicklen, J., 1959, The fluorescence and phosphorescence of biacetyl and acetone vapor, *J. Am. Chem. Soc.* 81, 3863–3866.

Kirk, A. D., and Porter, G. B., 1962, Kinetics of excited molecules. III Photo-oxidation of acetone, *J. Phys. Chem.* 66, 556–557.

Lee, E. K. C., and Lewis, R. S., 1980, Photochemistry of simple aldehydes and ketones in the gas phase, *Adv. Photochem.* 12, 1–98.

Marcotte, F. B. and Noyes, W. A. Jr., 1951, The reactions of radicals from acetone and oxygen, *Disc. Faraday Soc.* 10, 236–241.

Moortgat, G. K., and Warneck, P., 1979, CO and H_2 quantum yields in the photodecomposition of formaldehyde in air, *J. Chem. Phys.* 70, 3639–3651.

Niki, H., Maker, P. D., Savage, C. M., and Breitenbach, L. P., 1980, Further IR spectroscopic evidence for the formation of $CH_2(OH)OOH$ in the gas phase reaction of HO_2 with CH_2O, *Chem. Phys. Lett.* 75, 533–535.

Noyes, W. A., Porter, G. B., and Jolley, J. E., 1956, Primary photochemical processes in ketones, *Chem. Revs.* 56, 49–94.

Noyes, W. A., Duncan, A. B. F., and Manning, W. M., 1934, Photochemical studies XIX The ultraviolet absorption spectrum of acetone vapor, *J. Chem. Phys.* 2, 717–725.

Norrish, R. G. W., Crone, H. G., and Saltmarsh, O. D., 1934, Primary photochemical reactions; Part V. The spectroscopy and photochemical decomposition of acetone, *J. Chem. Soc.* 1.934, 1456–1464.

Osborne, A. D., Pitts, J. N. Jr., and Fowler, S. L., 1961, Investigations of the photo-oxidation of acetone at 3130. A using infrared analysis, *J. Phys. Chem.* 65, 1622–1625.

Pearson, G. S., 1963, The photo-oxidation of acetone, *J. Phys. Chem.* 67, 1686–1692.

Penkett, S. A., 1982, Non-methane organics in the remote troposphere, in E. D. Goldberg (ed.) *Atmospheric Chemistry, Dahlem Konference*, Springer-Verlag, Berlin, pp. 329–355.

Peterson, J. T., 1976, Calculated actinic fluxes (290–700 nm) for air pollution photochemistry applications, U.S. Environmental Protection Agency EPA-600/4-76-025, Environmental Sciences Research Laboratory, Research Triangle Park, N.C. pp. 55.

Rhäsa, D., Lorenz, K., and Zellner, R., 1984, private communication.

Rebbert, R. E., and Ausloos, P., 1964, Triplet state energy transfer from acetone to aliphatic aldehydes in the gas phase, *J. Am. Chem. Soc.* 86, 4803–4807.

Rebbert, R. E., and Ausloos, P., 1965, Quenching of the triplet state of acetone and biacetyl by various unsaturated hydrocarbons, *J. Am. Chem. Soc.* 87, 5569–5572.

Singh, H. B., and Hanst, P. L., 1981, Peroxyacetyl nitrate (PAN) in the unpolluted atmosphere: an important reservoir for nitrogen oxides, *Geophys. Res. Lett.* 8, 941–944.

Su, F., Calvert, J. G., and Shaw, J. H., 1979, Mechanism of the photo-oxidation of formaldehyde, *J. Phys. Chem.* 83, 3185–3191.

Veyret, B., Rayez, J. C., and Lesclaux, R., 1982, Mechanism of the photooxidation of formaldehyde studied by flash photolysis of CH_2O–O_2–NO_2 mixtures, *J. Phys. Chem.* 86, 3424–3430.

Zetzsch, C., 1982, Rate constants for the reactions of OH with acetone and methylethyl ketone in the gas phase, *7th Int. Symp. Gas Kinet.* 23–27 Aug., 1982, Göttingen, Germany, pp. 73–75.